Electronic Supplementary Material (ESI) for Dalton Transactions.

Supporting information

Highly Dispersed Co Anchored on Ce-doped Hydroxyapatite as a Dual-Functional Catalyst for Selective Hydrogenolysis of 5-Hydroxymethylfurfural

Zhuoyou Gao [a], Mengying Wang [a], Ningzhao Shang [a], Wei Gao [a], Xiang Cheng [a], Shutao Gao [a], Yongjun Gao [b,*], Chun Wang [a,*]

[a] College of Science, Hebei Agricultural University, Baoding 071001, China

[b] College of Chemical and Environmental Science, Hebei University, Baoding 071001, China

Catalyst Characterization

The high-resolution transmission electron microscopy (HRTEM) were acquired on JEOL model JEM-2011IJHR) at 200 kV with an electron acceleration energy of 200 kV to observe the size and morphology of the catalysts. The X-ray diffraction (XRD) patterns of the catalyst were collected at a Rigaku D/max 2500 X-ray diffractometer using Cu Kα radiation (40 kV, 150 mA). XPS analysis was performed on an ESCALAB 250 X-ray photoelectron spectrometer (Thermo, USA) equipped with Al Kα monochromatized radiation at 1486.6 eV X-ray source. The samples were pressed and attached to the sample tray. The samples were put into the instrument sample chamber. When the pressure of the samples chamber was less than 2.0×10^{-7} mbar, the samples were sent to the analysis chamber, the spot size was 500 μm, the working voltage was 12 kV, and the filament current was 6 mA. Full spectrum scanning energy 150 eV, step size 1 eV, the narrow-spectrum scan has a bandwidth of 30 eV and a step size of 0.1 eV. The data were calibrated by the internal standard method, using the binding energy of C 1s (284.8 eV) of the most common organic pollution carbon in the vacuum system as the reference peak. The surface area, total pore volume and pore size distribution of the catalyst were measured at -196^{o}C using N_2 adsorption with V-Sorb 2800P volumetric adsorption equipment (Jinaipu, China). The specific surface area was calculated using the Brunauer-Emmett-Teller (BET) method, and the pore size distributions were measured using Barrett-Joyner-Halenda (BJH) analysis from the desorption branch of the isotherms. The metal content of the materials was analyzed by a T.J.A. ICP-9000 type inductively coupled plasma optical emission spectroscopy (ICP-OES) instrument. Fourier-transform infrared spectra (FT-IR) were recorded on a Bruker Tensor 27 spectrometer at room temperature. The samples were finely ground and dispersed in KBr to make pellets for FT-IR characterizations. All spectra were recorded in the range of 4000-400 cm^{-1} with a resolution of 4 cm^{-1}. Ultraviolet-visible-near infrared diffuse reflectance spectroscopy (UV-vis-NIR DRS) was obtained with a SHIMADZU UV-2600 spectrometer in which $BaSO_4$ powder was used as the internal standard to obtain the oxidation

states of Co and Ce. The data were processed by the Kubelka-Munk function, which displayed in absorbance.

Analysis of HMF by GC-FID

Product analysis was carried out on a Shimazdu 2014C series gas chromatograph (GC) equipped with a flame ionization detector (FID). All the separations were performed on a HP-5 capillary column (30 m × 0.32 mm i.d. × 0.25 μm film thickness).

Conditions: 1 min hold at 60°C, heating rate 20°C/min from 60°C to 270°C, 3 min hold at 270°C; Injector: 250°C; Detector: FID, 280°C.

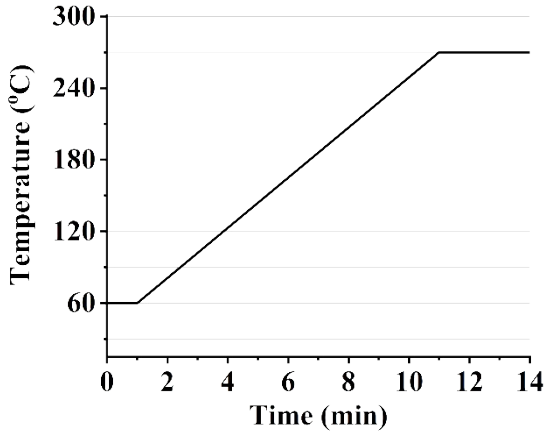

Temperature profile for GC analysis.

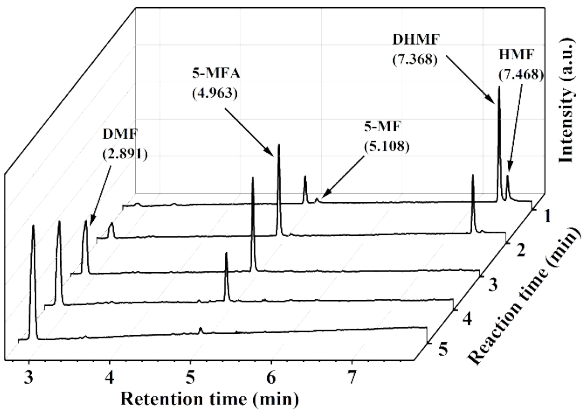

GC-FID chromatograms of the liquid products obtained from the selective hydrogenation of HMF over Co/HAP(Ce) at different times.

Calculation of the conversion and selectivity

The conversion and selectivity of DMF were calculated by the following equations:

$$\text{Conversion (\%)} = \frac{\text{moles of reactant reacted}}{\text{moles of reactant fed}} \times 100\%$$

$$\text{Selectivity (\%)} = \frac{\text{moles of product formed}}{\text{moles of reactant reacted}} \times 100\%$$

$$\text{Yield (\%)} = \frac{\text{moles of product formed}}{\text{moles of reactant fed}} \times 100\%$$

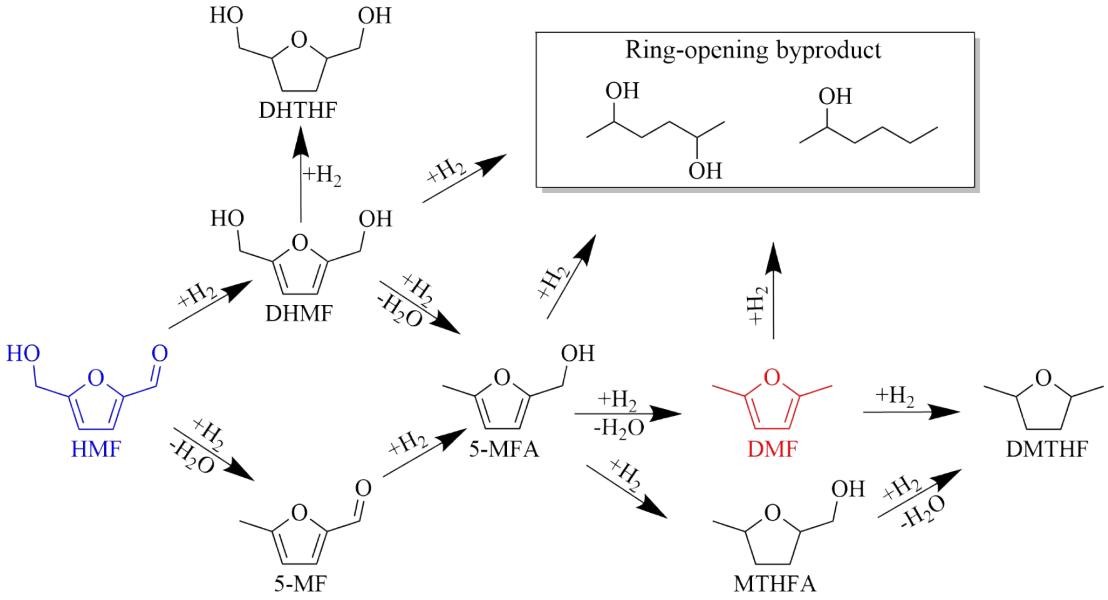

Figure S1. Network of products for selective hydrogenation of HMF

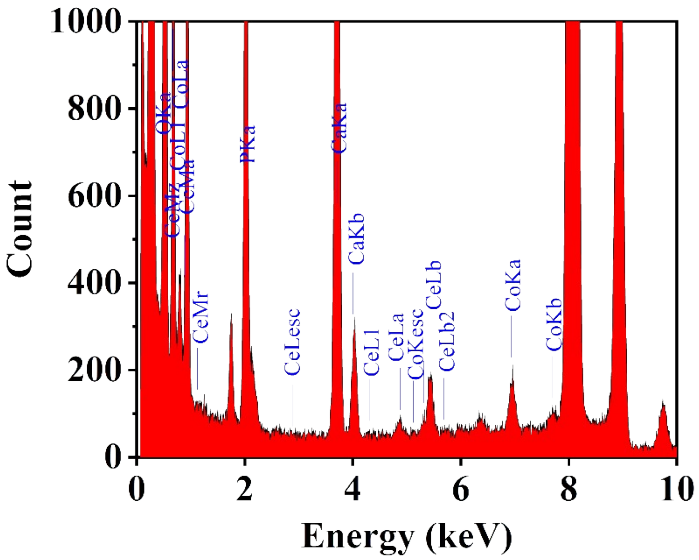

Figure S2. EDX of Co/HAP(Ce).

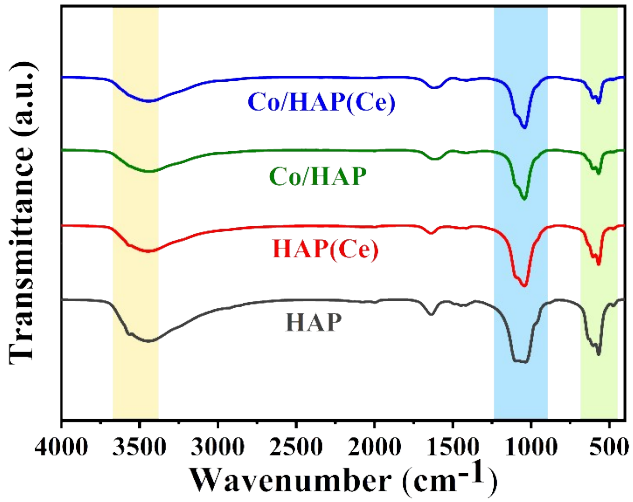

Figure S3. FT-IR spectra of different catalysts.

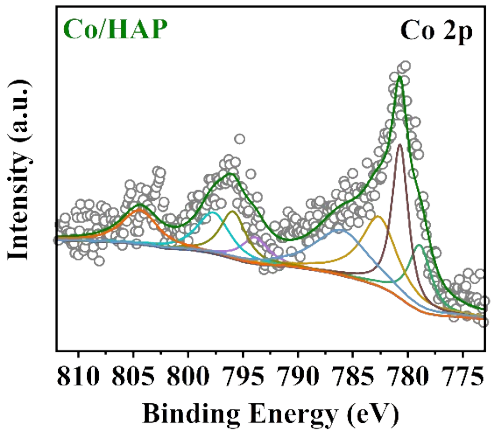

Figure S4. XPS characterization of Co 2p of Co/HAP.

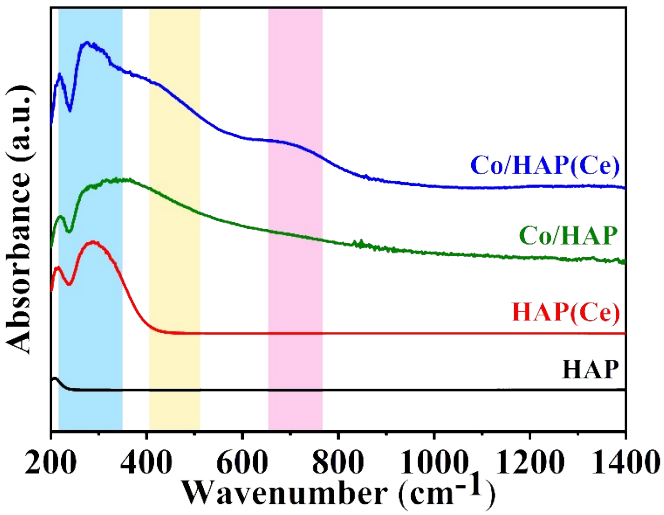

Figure S5. UV-VIS-NIR spectra of the catalysts.

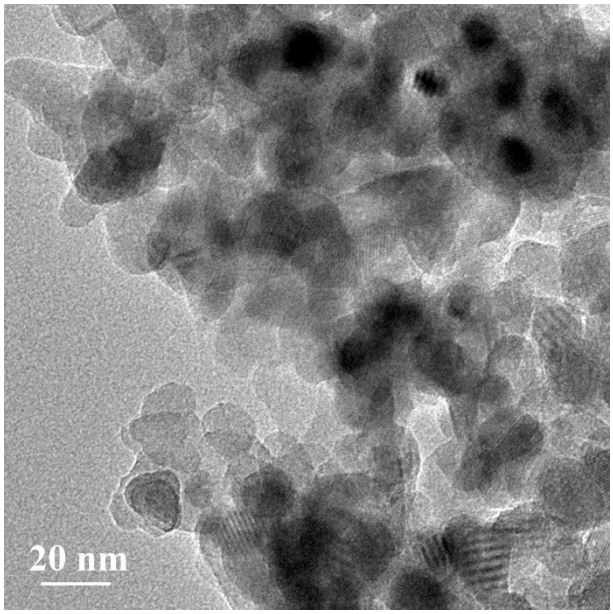

Figure S6. TEM image of the Co/HAP.

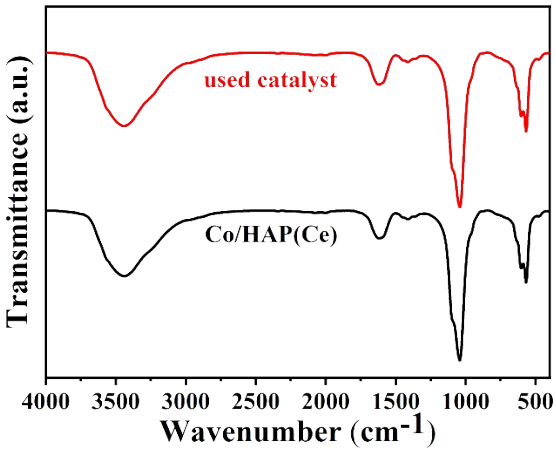

Figure S7. FT-IR spectra of the fresh and used catalyst.

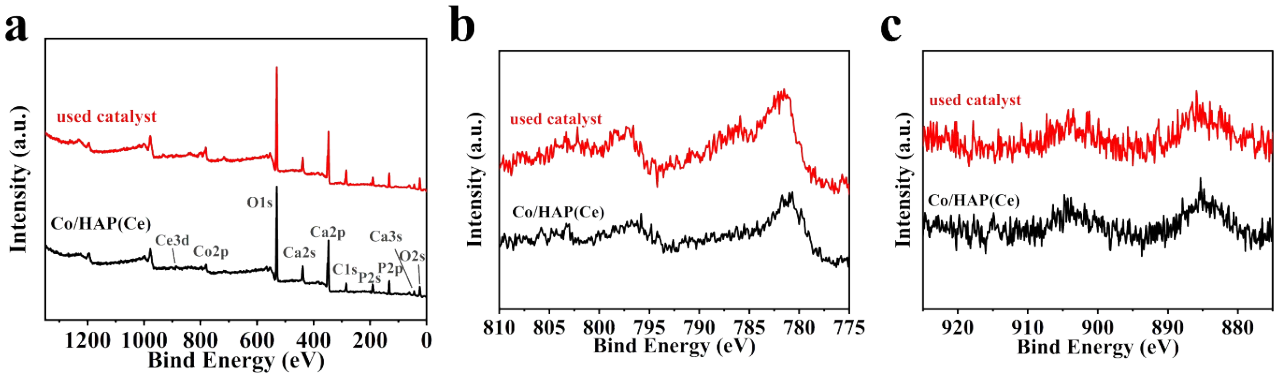

Figure S8. XPS scan spectra of the fresh and used catalyst (a), Co 2p (b), Ce 3d (c) spectra.

Table S1. Comparison of noble meatal catalysts for the HDO of HMF to DMF.

Entry	Catalyst	Solvent	T /°C	H_2 Pressure /MPa	Time /h	Yield /%	Reported year	Ref.
1	Pd/C/Zn	THF	150	0.8	8	85	2014	[1]
2	Ru/Co_3O_4	THF	130	0.7	24	93.4	2014	[2]
3	Pd/C + HCl PdAu/C + HCl	THF	60	0.1	6	100	2014	[3]
4	Pd/C + FA	dixoane	120	0.2	15	95	2015	[4]
5	Pd-$Cs_{2.5}H_{0.5}PW_{12}O_{40}$/K-10 clay	THF	90	1	2	81.3	2016	[5]
6	$RuCo/CoO_x$	1,4-dioxane	200	0.5	2	98.5	2018	[6]
7	PtCo/MWCNTs	1-butanol	160	0.1	8	92.3	2018	[7]
8	Pd/C	isopropanol	170	2	4	98	2018	[8]
9	Ru/CNT	dioxane	150	2	1	83.5	2018	[9]
10	Pt_1/Co	THF	180	1	2	92.9	2020	[10]
11	Br-Pd/Al_2O_3	THF	30	0.5	6	96.1	2021	[11]

Table S2. Comparison of non-noble meatal catalysts for the HDO of HMF to DMF.

Entry	Catalyst	Solvent	Temp /°C	H_2 /MPa	Time /h	Yield /%	Reported year	Ref.
1	NiAl-850	1,4-dioxane	180	1.2	4	91.5	2015	[12]
2	Ni_2-Fe_1/CNTs	n-butanol	200	3	3	91.3	2015	[13]
3	CuZn-2	1,4-dioxane	220	1.5	5	91.8	2015	[14]
4	NiSi-PS	THF	150	1.5	3	64.1	2015	[15]
5	Ni-OMD3	H_2O	200	3	6	97.7	2016	[16]
6	$CuCo^R$/NGr/α-Al_2O_3	THF	180	2	16	>98	2016	[17]
7	Cu-Co@C	ethanol	180	5	8	99.4	2017	[18]
8	Co@Cu/3$CoAlO_x$	1,4-dioxane	180	1	5	98.5	2019	[19]
9	Co_3O_4	1,4-dioxane	170	1	12	83.3	2019	[20]
10	5%Cu-15%Ni/BC	THF	220	4	12	98.5	2019	[21]
11	$Fe_{0.8}Co_{3.0}Ni_{1.9}$/h-BN	THF	180	2	4.5	94	2020	[22]
12	5Ni-7MoS_2/mAl_2O_3	isopropanol	130	1	6	95	2020	[23]
13	Co@N1Gs-700	ethanol	200	2	6	94.6	2020	[24]
14	Cu/Al_2O_3	THF	150	2	10	93.9	2020	[25]
15	Co-N-C/NiAl-MMO	THF	170	1.5	6	99.9	2020	[26]
16	Cu/ZnO-Al_2O_3	THF	180	1.2	5	90.1	2020	[27]
17	Co/Mix-ZrO_2	THF	130	1	2	90.7	2021	[28]
18	CoSi-PS	THF	170	1.5	4	97.5	2022	[29]
19	Co/BN	THF	180	2	4	91.7	2022	[30]
20	Ni-Mn/AC	THF	180	2	4	98.5	2022	[31]
21	**Co/HAP(Ce)**	**THF**	**150**	**2**	**5**	**96**	**This work**	

Table S3. Surface area and pore size of the catalysts.

Entry	Catalyst	Surface area [a] (m^2/g)	Pore size (nm)		Pore volume (cm^3/g)	
			SF [b]	BJH [c]	SF [d]	BJH [e]
1	HAP	117.4	0.74	24.76	0.04	0.64
2	HAP(Ce)	110.8	1.02	24.16	0.05	0.56
3	Co/HAP(Ce)	77.1	1.1	22.21	0.03	0.43

[a] BET surface area. [b] SF Median pore width. [c] BJH Adsorptiom average pore width (4V/A). [d] SF micropore volume. [e] BJH Adsorption cumulative volume.

Calculation details

DFT calculations were carried out using the "Vienna ab initio simulation package" (VASP5.3) [32]. The Perdew-Burke-Ernzerhof (PBE) exchange-correlation functional was used within the spin-polarized generalized gradient approximation (GGA) [33].A plane-wave basis set was employed within the framework of the projector augmented wave (PAW) method [34]. In order to get accurate results, the cutoff was set to 400 eV. In all calculations, k-points were sampled in a 3×3×1 Monkhorst-Pack grid. The HAP (001) surface is chosen as the computational model. Periodic boundary conditions are used for all systems. All calculations are spin polarized. Considering the 4f states of the reduced cerium atoms with the on-site Coulomb interaction, the value of the Hubbard U terms was used effectively, and the U value were determined by the report in other studies, which the value for Ce 4f was set to 5.0 eV [35]. In this study, we chose three models to do the comparative calculation, HAP (001) with a vacuum space of 20 Å in the z direction was used to simulate the HAP catalyst surface which was enough to avoid interactions between periodic images. The stable relaxed configurations are the Co is adsorbed to the oxygen atoms of the HAP according to our testing calculations (Figure S8), it was denoted as Co/HAP [36]. The Ce atoms replace the Ca atoms in the HAP and the Co is adsorbed to the oxygen atoms, which was denoted as Co/HAP(Ce). Bader charge population analysis was employed to compute atomic charge and electron transfer in different systems.

The stability of adsorbed species can be described by the differential adsorption energy ΔE, which is defined as： $\Delta E_{ad} = E_{(surface+A^*)} - E_{(surface)} - E_A$

where E(surface+A*) is the total energy for the adsorbed species adsorbed on the catalysts surfaces, E(surface) refers to the catalysts surfaces, and EA is the energy for adsorbed species. The ΔE_{ad} was obtained from the ground state calculations. With this definition, a negative value indicates an exothermic adsorption.

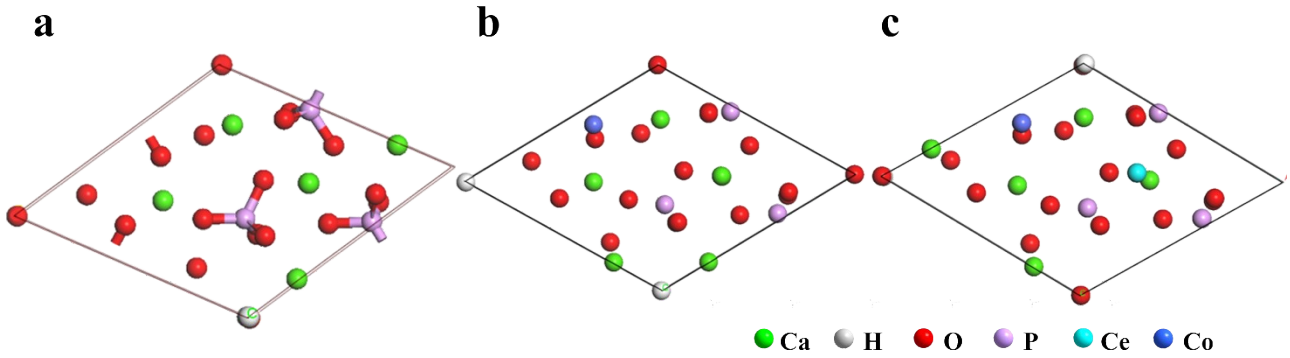

Figure S9. Optimized configuration of (a) HAP, (b) Co/HAP and (c) Co/HAP(Ce).

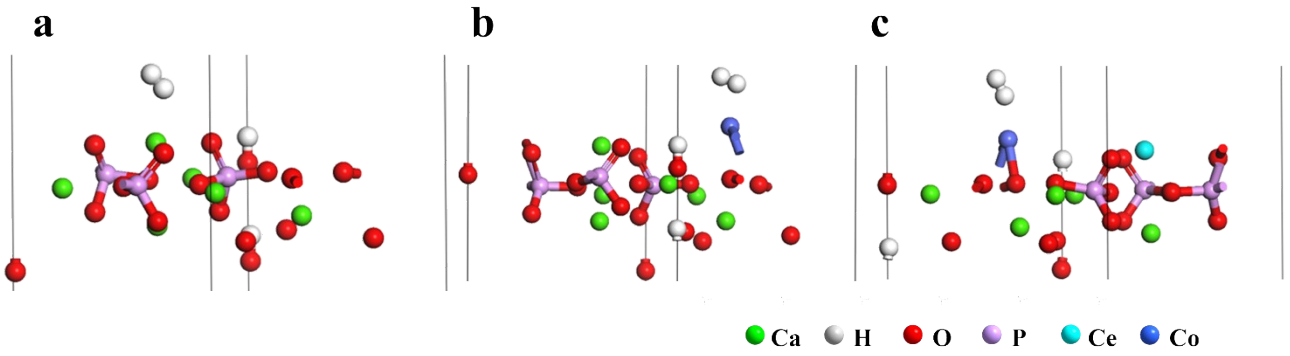

Figure S10. Optimized configurations of H_2 adsorbed on (a) HAP, (b) Co/HAP and (c) Co/HAP(Ce).

Table S4 Calculated adsorption energies of H_2 adsorbed on various active sites.

Species	ΔE_{ad}/eV		
	HAP	Co/HAP	Co/HAP(Ce)
H_2	-0.158	-1.35	-1.12
H		-3.15	-3.21

Table S5 Calculated bond length of H_2 or H adsorbed on the three sites

Entry	Item	H_2	HAP	Co/HAP	Co/HAP(Ce)
1	H-H bond length/Å	0.750	0.717	0.759	0.786
2	Co-H_2 bond length/Å			1.808	1.826

3	Co-H bond length/Å	1.553	1.563
4	H binding energy/eV	-1.826	-1.808

Table S6 Bader charge analysis of Co atom (e^-)

Atom	Co/HAP	Co/HAP(Ce)
Co	0.554	0.522
Ce		1.84

References:

1. B. Saha, C. M. Bohn and M. M. Abu-Omar, *ChemSusChem*, 2014, **7**, 3095-3101.
2. Y. Zu, P. Yang, J. Wang, X. Liu, J. Ren, G. Lu and Y. Wang, *Appl. Catal. B: Environ.*, 2014, **146**, 244-248.
3. S. Nishimura, N. Ikeda and K. Ebitani, *Catal. Today*, 2014, **232**, 89-98.
4. J. Mitra, X. Zhou and T. Rauchfuss, *Green Chem.*, 2015, **17**, 307-313.
5. A. B. Gawade, M. S. Tiwari and G. D. Yadav, *ACS Sustain. Chem. Eng.*, 2016, **4**, 4113-4123.
6. Z. Gao, G. Fan, M. Liu, L. Yang and F. Li, *Appl. Catal. B: Environ.*, 2018, **237**, 649-659.
7. X. Wang, Y. Liu and X. Liang, *Green Chem.*, 2018, **20**, 2894-2902.
8. B. S. Solanki and C. V. Rode, *Journal of Saudi Chemical Society*, 2019, **23**, 439-451.
9. P. Priecel, N. A. Endot, P. D. Carà and J. A. Lopez-Sanchez, *Ind Eng Chem Res*, 2018, **57**, 1991-2002.
10. T. Gan, Y. Liu, Q. He, H. Zhang, X. He and H. Ji, *ACS Sustain. Chem. Eng.*, 2020, **8**, 8692-8699.
11. D. Wu, S. Zhang, W. Y. Hernández, W. Baaziz, O. Ersen, M. Marinova, A. Y. Khodakov and V. V. Ordomsky, *ACS Catal.*, 2020, **11**, 19-30.
12. X. Kong, R. Zheng, Y. Zhu, G. Ding, Y. Zhu and Y.-W. Li, *Green Chem.*, 2015, **17**, 2504-2514.
13. L. Yu, L. He, J. Chen, J. Zheng, L. Ye, H. Lin and Y. Yuan, *ChemCatChem*, 2015, **7**, 1701-1707.
14. Y. Zhu, X. Kong, H. Zheng, G. Ding, Y. Zhu and Y.-W. Li, *Catal. Sci. Tech.*, 2015, **5**, 4208-4217.
15. X. Kong, Y. Zhu, H. Zheng, X. Li, Y. Zhu and Y.-W. Li, *ACS Catal.*, 2015, **5**, 5914-5920.
16. R. Goyal, B. Sarkar, A. Bag, N. Siddiqui, D. Dumbre, N. Lucas, S. K. Bhargava and A. Bordoloi, *J. Catal.*, 2016, **340**, 248-260.
17. W. Guo, H. Liu, S. Zhang, H. Han, H. Liu, T. Jiang, B. Han and T. Wu, *Green Chem.*, 2016, **18**, 6222-6228.
18. B. Chen, F. Li, Z. Huang and G. Yuan, *Appl. Catal. B: Environ.*, 2017, **200**, 192-199.
19. Q. Wang, J. Feng, L. Zheng, B. Wang, R. Bi, Y. He, H. Liu and D. Li, *ACS Catal.*, 2019, **10**, 1353-1365.
20. D. Li, Q. Liu, C. Zhu, H. Wang, C. Cui, C. Wang and L. Ma, *J.Energy Chem.*, 2019, **30**, 34-41.
21. C. Zhu, H. Wang, H. Li, B. Cai, W. Lv, C. Cai, C. Wang, L. Yan, Q. Liu and L. Ma, *ACS Sustain. Chem. Eng.*, 2019, **7**, 19556-19569.
22. N. Chen, Z. Zhu, T. Su, W. Liao, C. Deng, W. Ren, Y. Zhao and H. Lü, *Chem. Eng. J.*, 2020, **381**, 122755.
23. W. Han, M. Tang, J. Li, X. Li, J. Wang, L. Zhou, Y. Yang, Y. Wang and H. Ge, *Appl. Catal. B: Environ.*, 2020, **268**, 118748.
24. J. Wang, Q. Wei, Q. Ma, Z. Guo, F. Qin, Z. R. Ismagilov and W. Shen, *Appl. Catal. B: Environ.*, 2020, **263**, 118339.
25. L. M. Esteves, M. H. Brijaldo, E. G. Oliveira, J. J. Martinez, H. Rojas, A. Caytuero and F. B. Passos, *Fuel*, 2020, **270**, 117524.
26. N. Ma, Y. Song, F. Han, G. I. N. Waterhouse, Y. Li and S. Ai, *Catal. Sci. Tech.*, 2020, **10**, 4010-4018.
27. Q. Wang, Z. Yu, J. Feng, P. Fornasiero, Y. He and D. Li, *ACS Sustain. Chem. Eng.*, 2020, **8**, 15288-15298.
28. T. Xiao, X. Liu, G. Xu and Y. Zhang, *Appl. Catal. B: Environ.*, 2021, **295**, 120270.
29. L. Sun, S. Li, Z. Gao, S. Gao, W. Gao, X. Cheng, N. Shang, Y. Gao and C. Wang, *Dalton Trans.*, 2022, **51**, 3096-3103.
30. D. Bi, X. Chen, Z. Du, Z. Guo, Z. Liu, J. Lin, Y. Huang, C. Tang, G. Chen and Y. Fang, *ChemistrySelect*, 2022, **7**, e202104043.
31. Y. Liu, X. Shi, J. Hu, K. Liu, M. Zeng, Y. Hou and Z. Wei, *ChemSusChem*, 2022, DOI: 10.1002/cssc.202200193, e202200193.
32. J. P. Perdew, K. Burke and M. Ernzerhof, *Phys. Rev. Lett.*, 1996, **77**, 3865.
33. P. E. Blochl, *Phys. Rev. B*, 1994, **50**, 17953-17979.

34. K. G and J. D, *Phys.Rev. B*, 1999, **59**, 1758.
35. F. Yuan, R. Sun, L. Fu and G. Zhao, *Chin. Chem. Lett.*, 2022, **33**, 2188-2194.
36. S. Ding, Y. Guo, M. J. Hülsey, B. Zhang, H. Asakura, L. Liu, Y. Han, M. Gao, J.-y. Hasegawa, B. Qiao, T. Zhang and N. Yan, *Chem*, 2019, **5**, 3207-3219.